JOURNAL OF MATERIALS SCIENCE 31 (1996) 5429–5436

Analysis of local heat transfer properties of tape-cast AlN ceramics using photothermal reflectance microscopy

L. FABBRI, D. FOURNIER, L. POTTIER
Laboratoire d'Instrumentation, Université Pierre et Marie Curie; UPR A0005 du CNRS, 10 rue Vauquelin, 75005 Paris, France

L. ESPOSITO
CNR-IRTEC, Research Institute for Ceramics Technology, Faenza, Italy

Photothermal reflectance microscopy was applied to the analysis of local thermal diffusivity on tape-cast AlN ceramics. The materials were obtained from three different commercial powders, two sintering temperatures (1750 and 1800 °C), and 3 wt% Y_2O_3 sintering aid. Owing to the high spatial resolution of the technique ($\sim$30 μm in the present case), measurements in different positions on the sample surface were carried out. In this way a study of the homogeneity of thermal properties was performed.

1. Introduction

Aluminium nitride ceramics are excellent candidates for substrates of high-power and high-density integrated electronic packages. Alumina (Al_2O_3) is currently employed for substrate production, but its low thermal conductivity ($\sim 30\ W\,m^{-1}\,K^{-1}$ at 300 K [1, 2]) limits its use to low-power applications. Materials with higher conductivity, such as polycrystalline diamond, BeO, and BeO-based composites, are commercially available for advanced packaging devices in which the high dissipation of heat is required. Yet the high toxicity of BeO powders leads to several problems during substrate production. By contrast, AlN has a potentially high thermal conductivity, is non-toxic and often characterized by other interesting properties which make it an ideal candidate for electronic packaging: a low dielectric constant, high electrical resistivity, and a thermal expansion compatible to silicon [3–5]. The theoretical thermal conductivity of AlN for a pure single crystal has been estimated by Slack [6] to reach 320 $W\,m^{-1}\,K^{-1}$ at 300 K using the Leibfried–Sholomann scaling parameter and assuming that only intrinsic phonon–phonon scattering is effective. This value fixes an upper limit to the thermal conductivity of actual AlN, due to the detrimental effects of impurities (especially oxygen incorporated in the AlN lattice as dissolved $Al_{0.67}O$) [6]. This value was confirmed only recently by experimental work carried out on high-purity single-crystal AlN (oxygen content: $42 \pm 2 \times 10^8$ atoms cm^{-3}). The measured thermal conductivity was 285 $W\,m^{-1}\,K^{-1}$ at 300 K. The value corrected for the presence of oxygen was 319 $W\,m^{-1}\,K^{-1}$ [7].

Lower values have been found for polycrystalline ceramics, mainly due to the high oxygen contamination of AlN powders (typically 1 wt%). The use of different additives and processing conditions leads to a broad dispersion in the thermal properties of the final materials. This accounts for the large spread of data reported in the literature (60–270 $W\,m^{-1}\,K^{-1}$) [8–16].

Among different processing techniques, tape-casting is used largely to produce thin ceramic sheets (100–1000 μm) with smooth surfaces and accurate dimension tolerances [17], and has gained the manufacturer's interest for substrate production. Owing to the slight thickness of the samples produced according to this method, the application of the standard technique (laser-flash [18–20]) to measure thermal diffusivity, as well as the analysis of heat-transport properties, are far from straightforward. For instance, for samples with such geometry, it is very difficult to design a sample holder that would satisfy the laser-flash requirements (i.e. minimal thermal contact, and the suitable masking of the laser pulse). In addition, for slight thicknesses, non-uniform heating [21] and finite pulse effects [22] might be non-negligible. In spite of a few attempts to reduce the latter effect by shortening the laser pulse duration [23, 24], other problems still remain (e.g. excessive temperature gradient between front and back surfaces, which can result in a non-linear behaviour).

More recently, several techniques based on the photothermal effect (i.e. the generation of thermal waves by intensity-modulated optical excitation [25–28]) have been successfully applied to measure the thermal diffusivity of bulk materials [29, 30], of coatings [31, 32], and of thin films [33, 34]. As thermal waves are strongly damped within the materials, they furnish information on a spatial scale comparable to the thermal wavelength. The latter can be varied simply by changing the modulation frequency of the

0022–2461

heating beam. Regarding thermal wave propagation, even very thin samples can behave like a bulk, provided the modulation frequency is high enough.

Among photothermal techniques, photothermal reflectance microscopy (PRM) [35] has become particularly interesting as a microscopic tool for several applications, such as the characterization of material defects and interfaces [36, 37], the analysis of temperature distribution in diode lasers [38], and the study recombination processes in semiconductors [39, 40]. This is essentially due to its high spatial resolution: with the pump and probe beams focused down to the optical resolution limit, at high modulation frequencies (>1 MHz) thermal imaging can reach micronic resolution [35].

More recently, the PRM was successfully applied for the determination of the thermal diffusivity of solid materials by measuring the phase of the photothermal signal as a function of the pump-probe spacing [41–44]. Owing to the intrinsic high spatial resolution of PRM, local measurements can be performed. These measurements are particularly important for testing the homogeneity of the thermal properties of devices employed for micropackaging applications. In this work, local thermal diffusivity measurements were performed on a set of tape-cast AlN ceramics to investigate a possible dispersion in the thermal properties. Different samples obtained from three commercial powders at two sintering temperatures were studied.

2. Photothermal reflectance microscopy

The principle of the method consists in detecting the temperature distribution on the sample's surface through the variation of its reflection coefficient, R. Specifically, if an intensity modulated continuous wave (c.w.) laser beam is used as the heating source, the temperature rise, T, on the sample's surface is a function of the distance, r, from the heating centre. It has both a zero-frequency (d.c.) and harmonic (a.c.) components

$$T(r, t) = T_{\text{d.c.}}(r) + T_{\text{a.c.}}(r)\exp(-i\omega t) \tag{1}$$

with $i = (-1)^{1/2}$.

For a semi-infinite, homogeneous medium that is opaque to exciting radiation, assuming a gaussian distribution for the heating beam with $1/e$ radius a_h, the a.c.-temperature distribution has cylindrical symmetry, and can be expressed as an inverse Hankel transform [26, 27]

$$T_{\text{a.c.}}(r) = \int_0^\infty \bar{T}(\lambda)\exp\left(-\frac{\lambda^2 a_h^2}{4}\right)J_0(\lambda r)\lambda\,\mathrm{d}\lambda \tag{2a}$$

where

$$\bar{T}(\lambda) = \frac{P_h}{2\pi\kappa\sigma(\lambda)} \tag{2b}$$

Here κ is the sample's thermal conductivity, J_0 is the zero-order Bessel function of the first kind, P_h is the heating power and $\sigma(\lambda)$ is the thermal wave number

$$\sigma(\lambda) = \left(\lambda^2 + \frac{2i}{\mu^2}\right)^{1/2} \tag{3}$$

where $\mu = (2\alpha/\omega)^{1/2}$ is the thermal diffusion length (α is the thermal diffusivity).

The temperature rise on the surface therefore depends on the thermal properties of the sample through κ and $\sigma(\lambda)$. These quantities can be obtained through an inversion procedure. As mentioned above, the temperature rise can be detected through the reflectance variation on the sample's surface. The reflectance is related to the temperature as follows [35]

$$R(r, t) = R_0 + \frac{\mathrm{d}R}{\mathrm{d}T}T(r, t) \tag{4}$$

where R_0 is the reflectance at room temperature.

The a.c. component of the reflectance is evaluated by detecting the intensity variation of a probe beam reflected on the sample's surface. This is given by the convolution of R with the intensity distribution, I_p, of the probe beam before reflection

$$I_{\text{a.c.}}(\boldsymbol{r}) = \int_0^\infty R_{\text{a.c.}}(\boldsymbol{r}')I_p(\boldsymbol{r}' - \boldsymbol{r})\,\mathrm{d}^2\boldsymbol{r}' \tag{5}$$

where the centre of the heating beam is taken for the origin $\boldsymbol{r} = 0$. For a gaussian probe beam with power P_p, and $1/e$ radius a_p, due to the convolution properties of the Hankel transform, the following relation holds true

$$I_{\text{a.c.}}(r) = \frac{P_p P_h}{2(\pi a_p)^2\kappa}\frac{\mathrm{d}R}{\mathrm{d}T}\int_0^\infty \exp\left(-\frac{\lambda^2(a_p^2 + a_h^2)}{4}\right) \times \frac{J_0(\lambda r)}{\sigma(\lambda)}\lambda\,\mathrm{d}\lambda \tag{6}$$

where r is the distance between the centres of the heating and probe beams. Equations 2 and 6 show that the a.c. component of the reflected probe intensity is the same as would result from an "effective" temperature distribution, $T^*_{\text{a.c.}}$, produced on the same sample by a heating beam of gaussian radius $a_{\text{eff}} = (a_p^2 + a_h^2)^{1/2}$, and detected with a probe beam of radius equal to zero. This can be written as

$$I_{\text{a.c.}}(r) = \frac{P_p}{\pi a_p^2}\frac{\mathrm{d}R}{\mathrm{d}T}T^*_{\text{a.c.}}(r) \tag{7}$$

By studying the amplitude and the phase of $I_{\text{a.c.}}$ as functions of the offset, r, it is possible to measure the sample's thermal diffusivity after an inversion procedure. For this application, however, it is preferable to analyse the phase. The reason is that the phase, which is independent of any normalization, is much less affected by reflectance inhomogeneities, and does not explicitly depend on the power of the two beams.

As is well known, in the case of focused laser heating, the temperature distribution described by Equation 2 behaves asymptotically as a *spherical* thermal wave. In this case the phase of $I_{\text{a.c.}}$ is simply related to the offset r trough in linear relationship that involves only the thermal diffusion length, μ, of the

material [43].

$$\phi(r) = -\frac{r}{\mu} \tag{8}$$

In this way, by analysing the phase slope, it is possible to characterize the thermal diffusivity by the following relationship

$$\alpha = \frac{\omega}{2}\left[\frac{d\phi}{dr}(r)\right]^{-2} \tag{9}$$

The above approximation avoids the tedious problem of a genuine inversion procedure, typical of these techniques. A complete discussion of its validity for gaussian beams is reported elsewhere [45] where an error assessment was performed.

3. Experimental procedure

3.1. AlN materials

The samples were obtained using three commercial AlN powders: two of them produced by carbothermal reduction of Al_2O_3 (Atochem A4 and Tokuyama grade G) and the last one produced by direct nitridation of aluminium (Starck grade C). The green body of AlN was made by tape casting using a 3 wt % Y_2O_3 additive. The preparation of the tape-casting slurry was carried out by fast mixing the powder in a plastic jar with alumina balls with the proper solvents and organic additives, as described in detail elsewhere [46]. After casting and drying, a debonding cycle at 600 °C for the elimination of organic additives was carried out. For densification, the AlN green body was placed in a BN-lined graphite crucible using two different sintering temperatures (1750 and 1800 °C) with a 2 h soaking time. The AlN grain dimension of the final materials ranged between 3–4 μm and 4–5 μm for the sample processed at 1750 and 1800 °C, respectively (Fig. 1). The density of each sample (see Table I) was measured by using Archimedes' method. The porosity was roughly estimated from density data and by considering the theoretical density of Y_2O_3 and AlN phases (i.e. 5.01 and 3.26 g cm^{-3}, respectively).

Afterwards, the samples were coated with a thin film of gold (< 80 nm). This ensures both high reflectance for the red (670 nm) probe beam, and effective light-to-heat conversion of the high green (514 nm) heating beam on the sample's surface.

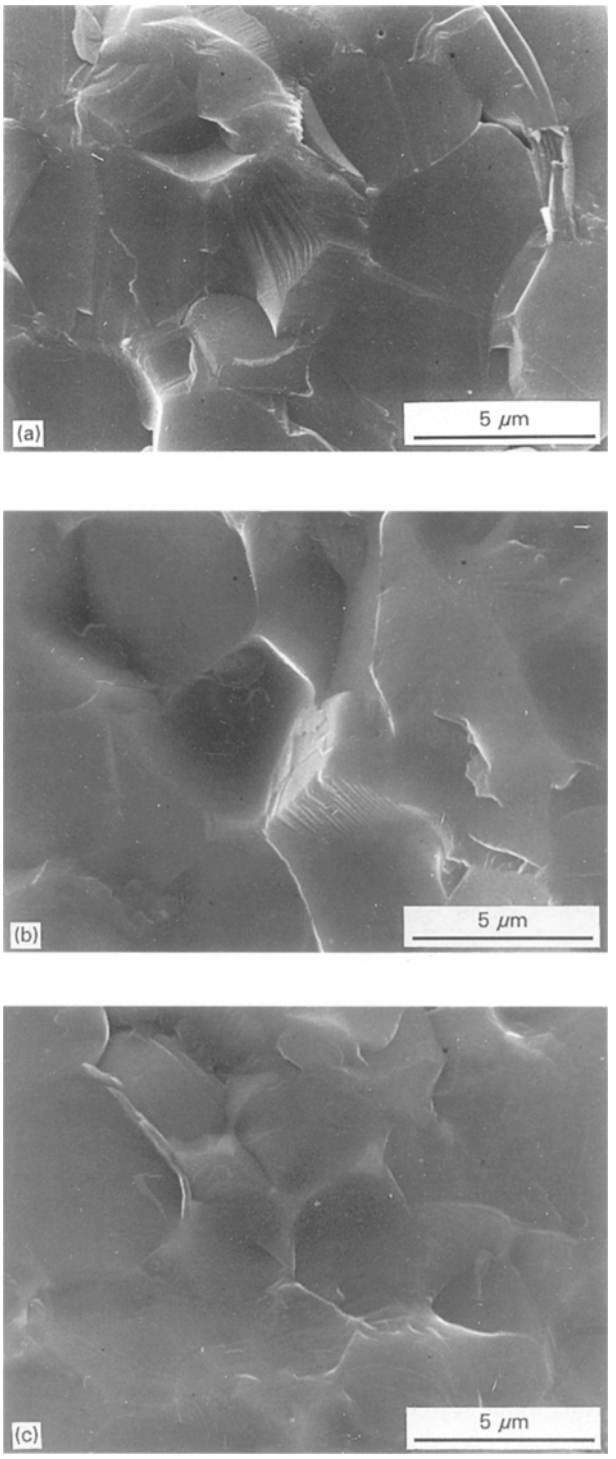

Figure 1 SEM microstructure of the fracture surface of the three AlN tapes sintered at 1800 °C for 2 h: (a) Atochem (A2); (b) Tokuyama (T2); (c) Starck (S2).

3.2. Apparatus

The experimental apparatus is shown in Fig. 2. The heating beam (Ar^+ laser, 514 nm) was intensity modulated by an acousto-optic device. Its power on the sample surface was always under 10 mW. The probe used to detect the reflectance variations was a GaAs diode laser (670 nm), with a power of about 1 mW on the sample surface. Both the beams were focused using an optical microscope down to the limit of resolution (1/*e* gaussian radius ~ 0.5 μm) after passing through its eyepiece and an objective (× 50, numerical aperture: $\phi = 0.75$). They were made collinear by a dichroic mirror driven by two stepping motors, so as to scan the sample's surface with the heating beam. In this way, it was possible to measure the photothermal signal as a function of the heating spot's position relative to the probe spot. As pointed out previously [41], keeping the probe fixed at a position that is a local (micronic) "good mirror" ensures both an efficient and geometrically clean reflection of the probe beam. Moving the heating spot on the possibly irregular surface of the inhomogeneous sample may result in erratic fluctuations of the amplitude, but leaves the phase unaffected. Furthermore, according to the reciprocity theorem for Green's functions of linear

TABLE I The materials studied

	Powder					
	A1 Atochem	T1 Tokuyama	S1 Starck	A2 Atochem	T2 Tokuyama	S2 Starck
T (°C)	1750	1750	1750	1800	1800	1800
t (h)	2	2	2	2	2	2
ρ (g cm^{-3})	3.26	3.26	3.27	3.28	3.28	3.27
P (%)	1.1	1.1	0.8	0.5	0.5	0.8

Main impurities (wt %)[a]	Atochem	Tokuyama	Starck
O	1.1	0.99	< 2.5
C	< 0.1	0.04	0.08
Fe	< 0.005	0.001	< 0.10

[a] Producer's data.

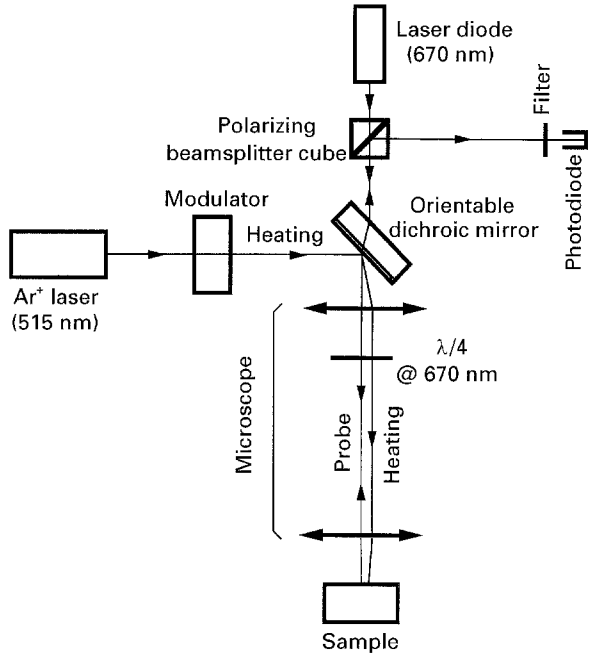

Figure 2 The experimental apparatus.

problems with homogeneous boundary conditions, the detected signal is the same as if the heating spots were fixed while the probe spot would be scanned. (In practice, it would be impossible to collect the reflected probe light, scattered by the sample's rugosity.) The observed phase distribution is thus the same as would be generated by a fixed heating spot.

The reflected probe beam was directed by an optical circulator (polarizing beamsplitter and birefringent plate that is quarterwave for the probe beam and is passed through twice) towards a fast low-noise silicon-detector. An optical filter was used to block residual radiation from the heating source. The signal was fed to a lock-in amplifier (EG&G 5302) to detect the amplitude and the phase of the fundamental Fourier component. The data were processed on-line by a PC connected through an IEEE-488 bus using an averaging procedure for noise reduction.

4. Results and discussion

The calibration of the experimental apparatus was made using an Armco iron sample as the reference material. Armco iron is currently used as a standard for thermal diffusivity measurements and has a value (0.205 cm^2 s^{-1} [47]) of the same order of magnitude of AlN ceramics. Its surface was carefully polished to obtain the high reflectance necessary for photoreflectance measurements. As the spatial resolution of our technique is very high (i.e. comparable to the thermal diffusion length), the measurements were performed at different locations on the surface in order to test the homogeneity of the material under study. More specifically, at different locations on the sample's surface, the phase of the photothermal signal was measured at a fixed modulation frequency ($f = \omega/2\pi$) of 10 kHz as a function of the relative coordinates (x, y) of the probe and heating beam centres. For the Armco iron this frequency corresponds to a thermal diffusion length of about 25 μm which roughly furnishes the size of the hemispherical region under investigation. A typical example of data output is shown in Fig. 3 where phase contour lines obtained at one location are displayed. These curves approach equi-spaced circles quite well because of the quasi-spherical nature of thermal waves which propagate in a material of reasonable homogeneity. The thermal diffusion length, μ, and, hence, the thermal diffusivity were determined using Equations 8 and 9, respectively, after reducing the experimental phase data as a function of the spacing $r = (x^2 + y^2)^{1/2}$. The slope calculation was made using the procedure described in [45]: as the a_{eff}/μ ratio was about 0.044, the theoretical error on μ is less than 1% if the slope is calculated after a distance r^* of about 6 μm. A point to note is that, under our experimental conditions, a temperature of about 100 K is produced on the sample surface at the heating beam centre. As the measurements are taken after a distance of 6 μm, an effective temperature of less than 10 K is expected. This means that our thermal diffusivity data are practically measured at room temperature.

The observed thermal diffusion length, μ, is defined as

$$\mu^{-1} = \frac{\phi(r^*) - \phi(r_{\max})}{r_{\max} - r^*} \tag{10}$$

where $r_{\max}$ is the maximum spacing for measurements to remain meaningful. Because the signal is a strongly

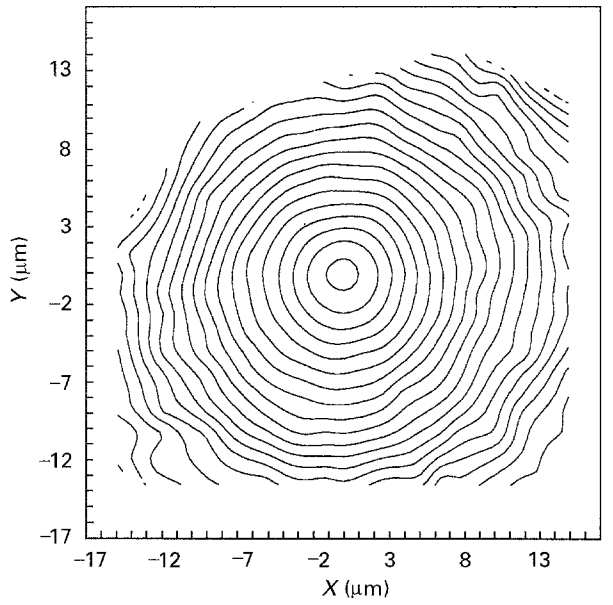

Figure 3 Phase map for Armco iron at one surface location (10 kHz). Equiphase curve spacing: 2°.

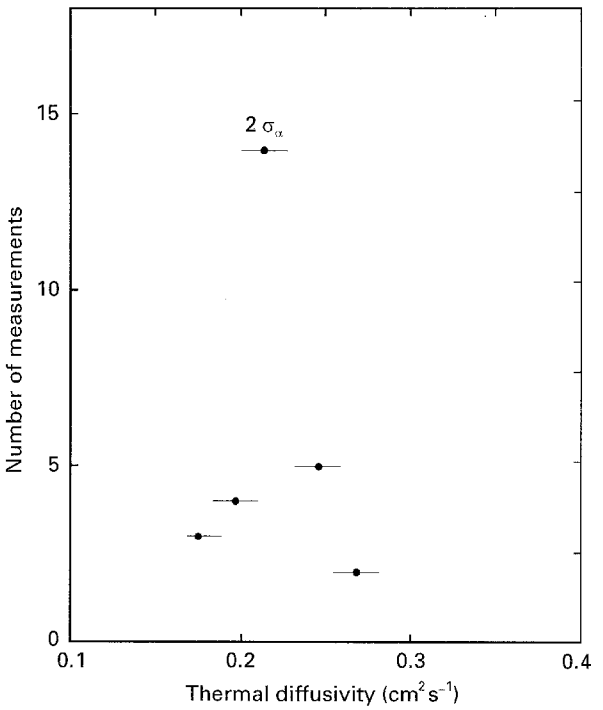

Figure 4 Thermal diffusivity data measured for 28 surface locations on Armco iron. Bar lengths: $\pm \sigma_\alpha$, σ_α being the α-standard deviation due to phase noise (Equation 11).

decreasing function of the spacing, $\phi(r_{max})$ is much noisier than $\phi(r^*)$. Consequently, a reasonable estimate on the uncertainty that affects μ due to noise, σ_μ, is given by:

$$\frac{\sigma_\mu}{\mu} = \frac{\sigma_\phi}{(r_{max} - r^*)}\mu \qquad (11)$$

where σ_ϕ is the maximum value of the phase standard deviation.

Typically, during the measurements at different locations on the different samples, the maximum distance, r_{max}, associated with an acceptable signal-to-noise ratio was about 20 μm. The corresponding standard deviation, σ_ϕ, of the phase was lower than 1°. These values correspond to a standard deviation, σ_μ/μ of about 3% for the thermal diffusion length, and, hence, of 6% for the thermal diffusivity (because $\sigma_\alpha/\alpha = 2\sigma_\mu/\mu$; see Equations 8 and 9).

In Fig. 4 the results obtained at different locations on the sample's surface are summarized. Each point represents the number of measurements with thermal diffusivity values falling within the interval identified by the $\pm \sigma_\alpha$-wide bar. The corresponding abscissa is the α mean value for the data falling in that interval. The distribution looks rather quite symmetrical: the average ($0.217\ cm^2\ s^{-1}$) and the median ($0.211\ cm^2\ s^{-1}$) differ from each other by less than 3%. The standard deviation, σ, of the whole data set is $0.0255\ cm^{-2}\ s^{-1}$, which is about twice the standard deviation related to the experimental noise. This demonstrates that a slight variation in the local thermal properties is present. Nevertheless, the average value ($0.217\ cm^2\ s^{-1}$) is very close to the bulk thermal diffusivity measured on the same sample using both the laser-flash method ($0.224\ cm^2\ s^{-1}$ [48]) and the "mirage" technique ($0.227\ cm^2\ s^{-1}$). This value also agrees quite well with the room-temperature TPRC value for the Armco iron ($0.205\ cm^2\ s^{-1}$ [47]) reported in the literature (i.e. with a scattering lower than 6%). These data also confirm that laser heating did not produce any noticeable variation of the average sample temperature.

Owing to the more complex microstructure of AlN ceramics, the measurements taken on AlN samples were less straightforward. The presence of different phases (mainly AlN and Y_2O_3) as well as possible resistance at the grain interfaces can generally cause scattering or reflection of thermal waves. These effects were considerably reduced by selecting a modulation frequency of 10 kHz. In fact, at 10 kHz, for materials with thermal diffusivity in the range 0.2–0.7 $cm^2\ s^{-1}$ the thermal diffusion length is 25–50 μm. This is about ten times greater than the grain size of our materials (i.e. 3–5 μm). A point to note is that each measurement is "localized in a hemisphere" whose radius is comparable with the value of μ. At 10 kHz, this hemisphere contains typically 10^2–10^3 AlN grains. It is thus representative of the local bulk properties. As the samples were available as tape-cast sheets with thicknesses of 500–800 μm, they behave like a semi-infinite medium for thermal waves propagation, which justifies the application of the theory described in Section 2.

The use of a thin gold film on the sample's surface was required to ensure good reflectivity of the probe beam, as well as efficient light-to-heat conversion of the heating beam on the sample's surface. The effect of the film on thermal wave propagation can be estimated from the three-dimensional theory for a two-layer system [26]. For instance, by assuming a thermal conductivity of 315 $W\ m^{-1}\ K^{-1}$ for the gold film (< 80 nm thick), the phase slope variation calculated at a spacing $r = \mu/2$ was below 2.5% in the worst case (i.e. $\alpha = 0.2\ cm^2\ s^{-1}$). Therefore, this effect can be generally neglected, and a correction was only applied to the lowest diffusivity data.

For each AlN sample, fifteen measurements on different surface points were carried out using the same procedure as employed for the Armco iron. The maximum value of the spacing was generally lower or equal to the thermal diffusion length of the material (~ 30 μm). The measured standard deviation, σ_α, was always about 5% of the mean value. The final results are summarized in Figs 5–7 and Table II where the

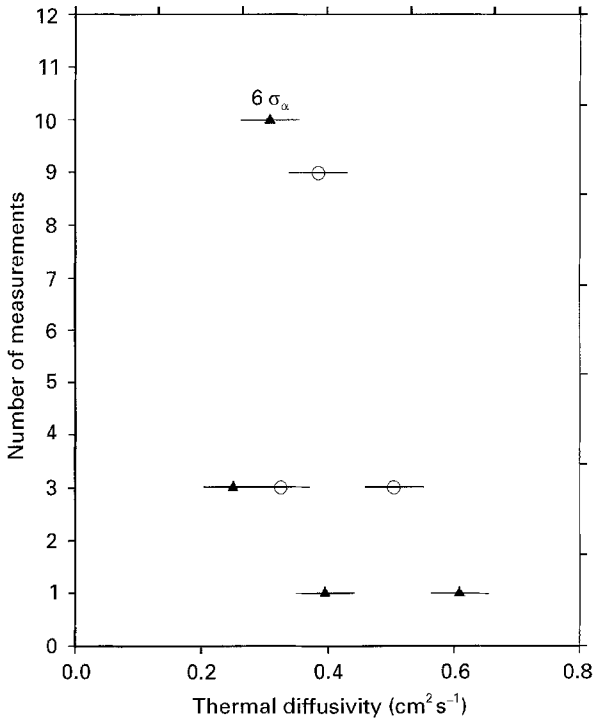

Figure 5 Thermal diffusivity data measured for 15 surface locations on sample processed from Atochem powders. (▲) A1 (1750 °C) and (○) A2 (1800 °C) samples.

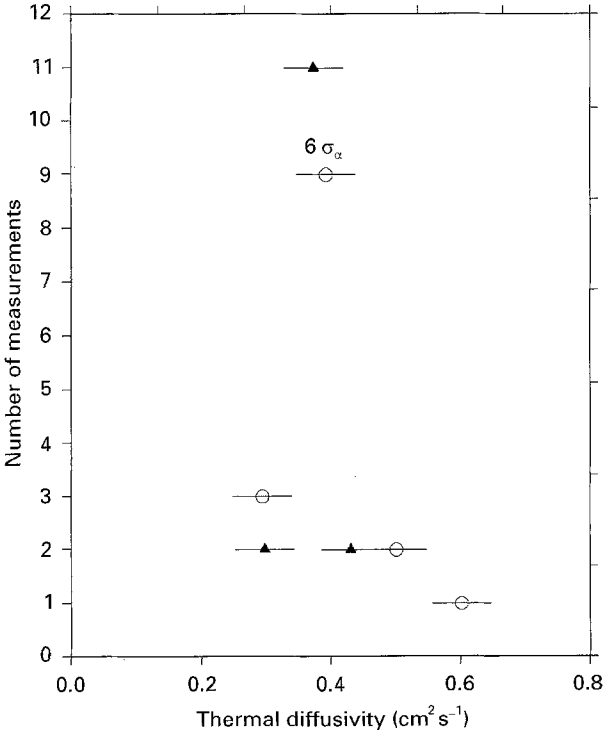

Figure 6 As Fig. 5 but for materials processed from Tokuyama powders. (▲) T1 (1750 °C) and (○) T2 (1800 °C) samples.

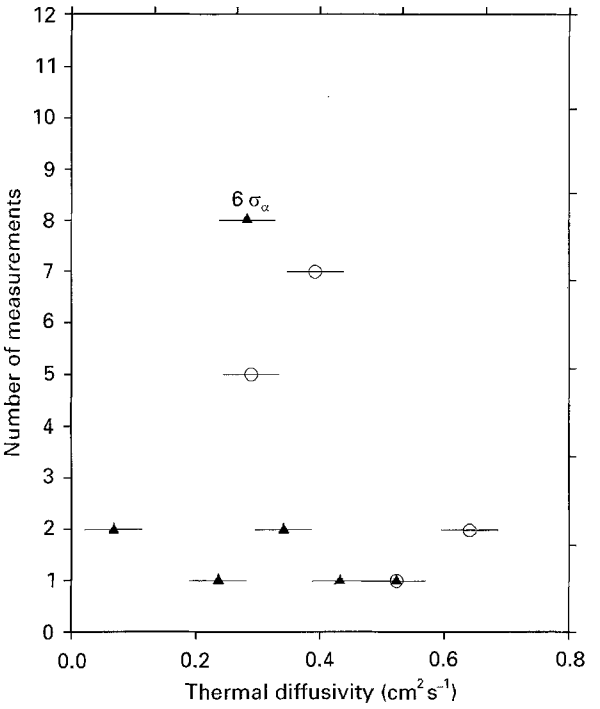

Figure 7 As Fig. 5, but for materials processed from Starck powders. (▲) S1 (1750 °C) and (○) S2 (1800 °C) samples.

average values obtained for each sample are reported. The thermal conductivity was calculated by using the well-known relationship

$$\kappa = \rho c_p \alpha \tag{12}$$

and the density data of Table I. The specific heat was calculated using the mixture law and literature values for the AlN and Y_2O_3 phases [49]. Fig. 5 shows the distribution of thermal diffusivity data for the samples processed with Atochem powders at different sintering temperatures (samples A1 and A2). As about 30% of the data scatter from the more populated bar, a significant variation of the thermal properties can be inferred between these two cases. A similar situation was present for the materials obtained from Tokuyama powers (Fig 6, T1 and T2 samples) while greater variations were found for Starck materials (samples: S1 and S2) as shown in Fig. 7. This was confirmed also by phase maps obtained on individual locations. Fig. 8 shows a typical phase map for the sample A1. Here, the equiphase curves present reasonable circular symmetry, showing this area to be relatively homogeneous. By contrast, the S2 material was often characterized by a deformation of equiphase curves as shown in Fig. 9. In this case, the variable spacing between equiphase curves is associated with the high inhomogeneity of the thermal properties. As is well known, the main factor controlling the thermal conductivity of AlN grains is the presence of impurities (mainly oxygen) in the crystal lattice [6–7, 9]. By contrast, the effect of porosity ($\sim 1\%$) and secondary phases (< 2 vol %) on heat-transfer properties can be considered completely irrelevant in the present case due to their very low volume fractions. Thus, the different behaviour found for our materials suggests that the amount and distribution of impurities may be

TABLE II Experimental results

	Powder					
	A1 Atochem	T1 Tokuyama	S1 Starck	A2 Atochem	T2 Tokuyama	S2 Starck
μ (μm) at 10 kHz	32.1	34.3	30.1	35.6	35.7	35.7
α ($cm^2 s^{-1}$)	0.323	0.370	0.284	0.397	0.401	0.400
α_{max} ($cm^2 s^{-1}$)	0.607	0.435	0.523	0.531	0.602	0.69
α_{min} ($cm^2 s^{-1}$)	0.214	0.292	0.061	0.317	0.284	0.256
κ ($W m^{-1} K^{-1}$)	81	93	71	101	102	101

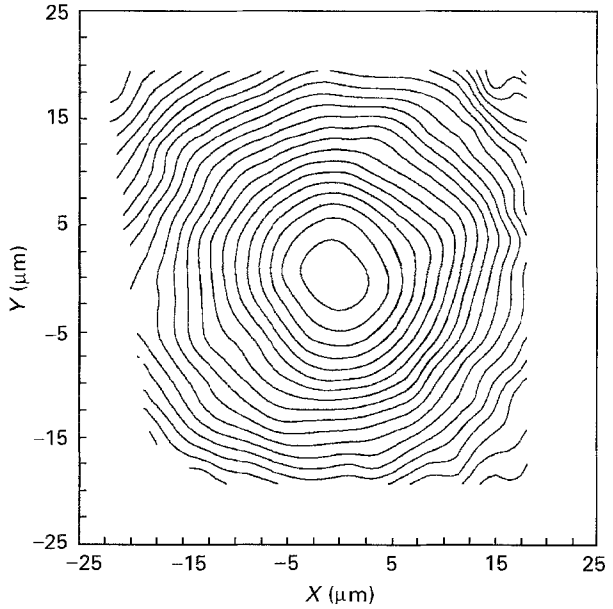

Figure 8 Phase map for sample A1 at one surface location (10 kHz). The 2° spaced equiphase curves present reasonable circular symmetry.

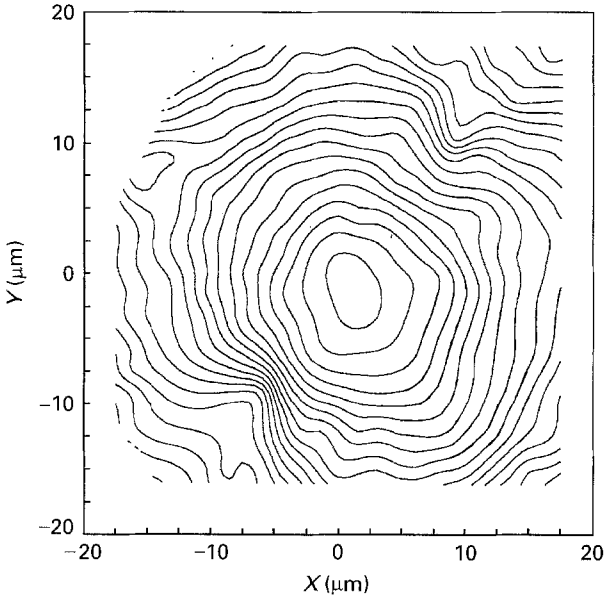

Figure 9 Phase map for sample S2 at one surface location (10 kHz). The deformation of the equiphase curve (2° spaced) is obvious. It indicates some diffusivity disorder (inhomogeneity, anisotropy).

different in the examined cases. In fact, Starck powders are less pure than the others (see Table I) which accounts for the lower data found for the S1 sample. By contrast, the sample T1 was processed using purer Tokuyama powder and has the highest values of thermal conductivity among the samples sintered at 1750 °C.

For each material, a slight increase in thermal diffusivity with sintering temperature is observed. This is a well-known effect associated with the presence of the Y_2O_3 phase which acts as an impurity trap for the oxygen present in the AlN grains [9]. The purification of AlN grains from oxygen considerably reduces the phonon scattering with a consequent increase in the thermal transfer properties. Although the mechanisms of oxygen removal are not completely understood [50], this phenomenon is, however, promoted by the temperature and it is reasonable to assume that it acts in different way for samples prepared from powders of different purities. The average data for thermal conductivity (Table II) agree quite well with those reported in the literature for similar materials obtained from the same powders but different forming techniques [14]. However, in view of its greater purity, the sample T2 shows an average value that is considerably lower than the expected one (about 20% less).

5. Conclusions

Local measurements of thermal diffusivity were performed by using photothermal reflectance microscopy. The calibration of the experimental equipment was made on an Armco iron sample. The result agree to within 6% with laser-flash or "mirage" data, as well as with the values taken from the literature.

For the AlN materials processed with powders having a different starting level of purity, a different dispersion of data was found. This is probably due to different oxygen distribution within the AlN grains. The samples processed at higher temperature (1800 °C) had the same average thermal conductivity regardless of the purity of the starting powders. Nevertheless, a thorough comparison with similar materials is not yet possible in view of the present lack of data concerning tape-case ceramics.

Acknowledgements

We thank Professor A. C. Boccara and Dr A. Bellosi for many fruitful scientific discussions. L. F. acknowledges EC funding for a postdoctoral grant obtained in the context of the "Human Capital and Mobility" project.

References

1. R. W. WILLIAMS, R. S. GRAVES, M. A. JANNEY, T. N. TIEGS and D. W. YARBROUGH, *J. Appl. Phys.* **61** (1987) 4894.
2. L. FABBRI, E. SCAFÈ and G. DINELLI, *J. Eur. Ceram. Soc.* **14** (1994) 441.
3. K. SHINOZAKI, N. IWASE and A. TSUGE, FC Annual Report, Toshiba Research and Development Center, Toshiba Corp. (1986) p. 16.
4. T. J. MORZ, *Ceram. Bull.* **70** (1991) 848.
5. L. M. SHEPPARD, *Am. Ceram. Soc. Bull.* **69** (1990) 1801.
6. G. A. SLACK, *J. Phys. Chem. Solids* **34** (1973) 321.
7. G. A. SLACK, R. A. TANZILLI, R. O. POHL and J. W. VANDERSANDE, *ibid.* **48** (1987) 641.
8. K. KOMEYA, *J. Am. Ceram. Soc.* **63** (1984) 1158.
9. A. V. VIRKAR, T. B. JACKSON and R. A. CUTLER, *ibid.* **72** (1989) 2031.
10. N. KURAMOTO, H. TANIGUCHI and I. ASO, *Am. Ceram. Soc. Bull.* **68** (1989) 883.
11. R. R. LEE, *J. Am. Ceram. Soc.* **74** (1991) 2242.
12. T. B. JACKSON, K. D. DONALDSON and D. P. H. HASSELMAN, *ibid.* **73** (1990) 2511.
13. K. WATARI, M. KAWAMOTO and K. ISHIZAKI, *J. Mater. Sci.* **26** (1991) 4727.
14. A. BELLOSI, L. ESPOSITO, E. SCAFÈ and L. FABBRI, *ibid.* **29** (1994) 5014.
15. P. SAINZ. de BARANDA, A. K. KNUDSEN and E. RUH, *J. Am. Ceram. Soc.* **77** (1994) 1846.
16. K. KOMEYA, *ibid.* **63** (1984) 1158.
17. P. BOCH and T. CHARTIER, *Ceram. For. Int.* **4** (1989) 55.
18. W. J. PARKER, R. J. JENKINS, C. P. BUTLER and G. L. ABBOT, *J. Appl. Phys.* **32** (1961) 1979.
19. ASTM C714-72, "Standard test method for thermal diffusivity of carbon and graphite by a thermal pulse method", American Society for Testing and Materials, Philadelphia, PA, 1972).
20. BS 7134: Section 4.2: 1990, "Testing of engineering ceramics: Method for the determination of thermal diffusivity by the laser flash (or heat pulse) method" (British Standards Institution, London, 1990).
21. L. FABBRI and E. SCAFÈ, *Rev. Sci. Instrum.* **63** (1992) 2008; Erratum, *ibid.* **65** (1994) 3594.
22. J. A. CAPE and G. W. LEHMAN, *J. Appl. Phys.* **34** (1963) 1909.
23. T. D. SIMS, in "Thermal Conductivity", Vol. 21, edited by C. J. Cremers and H. A. Fine (Plenum Press, New York, 1990) p. 133.
24. D. P. H. HASSELMAN, Virginia Polytechnic Institute, private communication (1995).
25. W. B. JACKSON, N. M. AMER, C. BOCCARA and D. FOURNIER, *Appl. Opt.* **20** (1981) 1333.
26. L. C. AAMODT and J. C. MURPHY, *J. Appl. Phys.* **52** (1981) 4903.
27. J. OPSAL and A. ROSENCWAIG, *ibid.* **53** (1982) 4240.
28. A. ROSENCWAIG, *Science* **218** (1982) 223.
29. G. ROUSSET and F. LEPOUTRE, *Rev. Phys. Appl.* **17** (1982) 201.
30. P. K. KUO, E. D. SENDLER, L. F. FAVRO and R. L. THOMAS, *Can. J. Phys.* **64** (1986) 1168.
31. P. M. PATEL and D. P. ALMOND, *J. Mater. Sci.* **20** (1985) 955.
32. H. P. R. FREDERIKSE, X. T. YING and A. FELDMAN, in "Proceedings of the Materials Research Society Symposium", Vol. 142, edited by J. Holbrook and J. Bussiere (MRS, Boston, 1989) p. 289.
33. A. SKUMANICH, H. DERSCH, M. FATHALLAH and N. M. AMER, *Appl. Phys. A* **43** (1987) 297.
34. J. P. ROGER, F. LEPOUTRE, D. FOURNIER and A. C. BOCCARA, *Thin Solid Films* **155** (1987) 174.
35. A. ROSENCWAIG, J. OPSAL, W. L. SMITH and D. L. WILLENBORG, *Appl. Phys. Lett.* **46** (1985) 1013.
36. F. LEPOUTRE, P. FORGE, F. C. CHEN and D. BALAGEAS, *La Recherche Aérospatiale* **1** (1994) 39.
37. A. M. MANSANARES, T. VELINOV, Z. BOZOKI, D. FOURNIER and A. C. BOCCARA, *J. Appl. Phys.* **75** (1994) 3344.
38. A. M. MANSANARES, J. P. ROGER, D. FOURNIER and A. C. BOCCARA, *Appl. Phys. Lett.* **64** (1994) 4.
39. W. L. SMITH, A. ROSENCWAIG and D. L. WILLENBORG, *ibid.* **47** (1985) 584.
40. L. J. INGLEHART, A. BRONIATOWNSKI, D. FOURNIER, A. C. BOCCARA and F. LEPOUTRE, *ibid.* **56** (1990) 1749.
41. L. POTTIER, *ibid.* **64** (1994) 1618.
42. D. FOURNIER, L. POTTIER, A. C. BOCCARA, G. SAVIGNAT, P. BOCH, J. POIRIER and G. PROVOST, "Advances in Science and Technology", Vol. 3A, edited by P. Vincenzini (Techna Srl, Firenze, 1995) p. 415.
43. C. PÉLISSONNIER, L. POTTIER, D. FOURNIER and A. THOREL, in "Proceedings of the European Ceramic Society Conference", Fourth Eurochem Vol. 3, edited by S. Nerrani and V. Sergo (Gruppo Editoriale Faeuza Editrice SpA, 1995) pp. 413–20.
44. A. SALAZAR and A. SANCHEZ-LAVEGA, *Rev. Sci. Instrum.* **65** (1994) 2896.
45. L. FABBRI and P. FENICI, *ibid.* **66** (1995) 3593.
46. L. ESPOSITO, A. BELLOSI and E. RONCARI, *Br. Ceram. Trns.*, **94** (1995) 1.
47. Y. S. TOULOUKIAN, R. W. POWELL, C. Y. HO and M. C. NICOULAOU, "Thermophysical Properties of Matter, Thermal Diffusivity", Vol. 10, TPRC Data Services (IFI/Plenum, New York, 1973).
48. L. GANDOSSI, Politecnico di Milano Italy, Tesi di Laurea "Misure di diffusivit termica su materiali di interesse areospaziale con tecnica ad impulso laser", February 1995.
49. LANDOLT-BÖRNSTEIN TABELLEN: "Eigenschaften der Materie in ihren Aggregatzuständen", Vol. 4, "Kalorische Zustandsgrössen" (Springer, Berlin, Göttingen, Heidelberg, 1961).
50. M. STERNITZKE and G. MÜLLER, *J. Am. Ceram. Soc.* **77** (1994) 737.

Received 30 August 1995
and accepted 24 April 1996